Clim. Past Discuss., 11, 5605–5649, 2015
www.clim-past-discuss.net/11/5605/2015/
doi:10.5194/cpd-11-5605-2015
© Author(s) 2015. CC Attribution 3.0 License.

Climate of the Past Discussions
Open Access
EGU

This discussion paper is/has been under review for the journal Climate of the Past (CP).
Please refer to the corresponding final paper in CP if available.

Regional climate signal vs. local noise: a two-dimensional view of water isotopes in Antarctic firn at Kohnen station, Dronning Maud Land

T. Münch[1,2], S. Kipfstuhl[3], J. Freitag[3], H. Meyer[1], and T. Laepple[1]

[1]Alfred Wegener Institute Helmholtz Centre for Polar and Marine Research, Telegrafenberg A43, 14473 Potsdam, Germany
[2]Institute of Physics and Astronomy, University of Potsdam, Karl-Liebknecht-Str. 24/25, 14476 Potsdam, Germany
[3]Alfred Wegener Institute Helmholtz Centre for Polar and Marine Research, Am Alten Hafen 26, 27568 Bremerhaven, Germany

Received: 13 October 2015 – Accepted: 5 November 2015 – Published: 26 November 2015

Correspondence to: T. Münch (tmuench@awi.de)

Published by Copernicus Publications on behalf of the European Geosciences Union.

Abstract

In low-accumulation regions, the reliability of δ^{18}O-derived temperature signals from ice cores within the Holocene is unclear, primarily due to small Holocene climate changes relative to the intrinsic noise of the isotopic signal. In order to learn about the representativity of single ice cores and to optimise future ice-core-based climate reconstructions, we studied the stable-water isotope composition of firn at Kohnen station, Dronning Maud Land, Antarctica. Analysing δ^{18}O in two 50 m long snow trenches allowed us to create an unprecedented, two-dimensional image characterising the isotopic variations from the centimetre to the hundred-metre scale. Our results show a clear seasonal layering of the isotopic composition, consistent with the accumulation rate, as well as high lateral isotopic variability caused by local stratigraphic noise. Based on the horizontal and vertical structure of the isotopic variations, we derive a statistical model for the stratigraphic noise. Our model successfully explains the trench data and allows to determine an upper bound of the reliability of climate reconstructions from seasonal to inter-annual time scales, depending on the number and the spacing of the cores taken. Implications for our study region include that reliably detecting a warming trend (0.1 °C decade^{-1}) in 50 years of data would require ∼ 10–50 replicate cores with a horizontal spacing of at least 10 m. More generally, our results suggest that in order to obtain high-resolution records of Holocene temperature change, fast measurements, thus allowing multiple cores, are more important than to minimise analytic uncertainty as the latter only plays a minor role in the total uncertainty.

1 Introduction

Ice cores obtained from continental ice sheets and glaciers are a key climate archive. They store information on past changes in temperature in the form of stable water isotopes (EPICA community members, 2006), in greenhouse gas concentrations via trapped air (Raynaud et al., 1993) and in many other parameters such as accumulation

CPD
11, 5605–5649, 2015

rates (e.g., Mosley-Thompson et al., 2001) or aerosols (e.g., Legrand and Mayewski, 1997).

The quantitative interpretation of stable water isotopes builds on the strong relationship between the isotopic ratios in precipitation and local air temperature (Dansgaard, 1964; Fujita and Abe, 2006). Analysis of the isotope ratios recorded in single deep ice cores provided milestones in the palaeo-climate research, including the investigation of glacial-interglacial climate changes (Petit et al., 1999) and the existence of rapid climate variations within glacial periods (Dansgaard et al., 1993).

In contrast to this coherent view from polar ice cores on millennial and longer time scales, the reliability of single ice cores as archives of the Holocene climate evolution is less clear (Kobashi et al., 2011). The small amplitude of Holocene climate changes and the aim to reconstruct them at a high temporal resolution poses a challenge to the interpretation of ice-core signals. This is especially true for low-accumulation sites as here the non-climate noise – to which we refer in this manuscript as the part of the isotopic record that cannot be interpreted in terms of large-scale temperature variations – may often be too high to accurately extract a climatic signal (Fisher et al., 1985). Despite the challenges, quantifying the Holocene polar climate variability is the key foundation to determine the range of possible future climate changes (e.g., Huntingford et al., 2013, and references therein) as well as to test the ability of climate models in simulating natural climate variability (Laepple and Huybers, 2014).

The quantitative estimation of climate variability from proxy data requires an understanding of non-climate influences in order to separate them from the climate signal (e.g., Laepple and Huybers, 2013). Several mechanisms influence the isotopic composition of snow prior to and after its deposition onto the ice sheet and thus cause non-climate noise in ice-core signals. Irregular deposition caused by wind and surface roughness along with spatial redistribution and erosion of snow is a major contribution to non-climate variance ("stratigraphic noise") (Fisher et al., 1985). Wind scouring can additionally remove entire seasons from the isotopic record (Fisher et al., 1983). Non-climate variability may further be introduced by spatial as well as temporal precip-

CPD
11, 5605–5649, 2015

itation intermittency (Persson et al., 2011; Sime et al., 2009, 2011). After deposition, vapour exchange with the atmosphere by sublimation-condensation processes (Steen-Larsen et al., 2014) can influence the isotopic composition of the surface layers; diffusion of vapour into or out of the firn driven by forced ventilation (Waddington et al., 2002; Neumann and Waddington, 2004; Town et al., 2008) may represent an additional component of post-depositional change. Finally, diffusion of water vapour through the porous firn smoothes isotopic variations from seasonal to inter-annual and possibly longer time scales, depending on the accumulation rate (Johnsen, 1977; Whillans and Grootes, 1985; Cuffey and Steig, 1998; Johnsen et al., 2000).

In the last two decades, a growing number of studies analysed to which extent single ice cores record a representative climate signal on sub-millennial time scales. One well-studied region is Dronning Maud Land (DML) on the East Antarctic Plateau. Comparing 16 annually resolved isotope records from DML spanning the last 200 years, Graf et al. (2002) found low signal-to-noise variance ratios of 0.14 for oxygen isotope ratios and 0.04 for accumulation rates. Karlöf et al. (2006) analysed 200 year-long records of oxygen isotopes and electrical properties in five cores with inter-site spacings of 3.5–7 km and detected no relationship between the cores except for volcanic imprints. This result is consistent with Sommer et al. (2000a, b) who studied high-resolution records of chemical trace species from three DML shallow ice cores (inter-site distances of $\sim$ 100–200 km) and discovered a lack of inter-site correlation on decadal time scales. Reconstructed accumulation rates showed a weak but significant correlation between two cores only on time scales larger than 30 years (Sommer et al., 2000a). The low representativity of single low-accumulation records was also supported by process studies comparing observed and simulated snow pits, the latter modelled by combining backward trajectories with a Rayleigh-type distillation model (Helsen et al., 2006). While the model-data comparison exercise was reasonably successful for coastal high-accumulation regions of DML, it largely failed on the dryer East Antarctic plateau. Such a relationship between accumulation rate and the signal-to-noise ratio of ice cores was further demonstrated in different studies across the Antarctic continent (Hoshina et al.,

CPD
11, 5605–5649, 2015

2014; Jones et al., 2014; McMorrow et al., 2002). A similar question of representativity also arises for Artic and Greenlandic records, although the higher accumulation rates generally lead to a higher signal content (Fisher and Koerner, 1994; Steen-Larsen et al., 2011; Gfeller et al., 2014).

Despite this large body of literature, quantitative information about the signal-to-noise ratios and the noise itself is mainly limited to correlation statistics of nearby cores. While a relatively good understanding of stratigraphic noise exists in Arctic records (Fisher et al., 1985), this does not apply to large parts of Antarctica where the environment is markedly different with the accumulation being considerably reworked in and between storms (Fisher et al., 1985).

Here we provide a direct visualisation and analysis of the signal and noise in an Antarctic low-accumulation region by an extensive two-dimensional sampling of the firn column in two 50 m long snow trenches. Our approach, for the first time, offers a detailed quantitative analysis of the spatial structure of isotope variability on a centimetre to hundred-metre scale. This is a first step towards a signal and noise model to enable quantitative reconstruction of the climate signal and its uncertainties from ice cores.

2 Data and methods

Near Kohnen station, close to the EPICA deep ice core drilling site on Dronning Maud Land (EDML, −75.0° S, 0.1° E, altitude 2892 m a.s.l., mean annual temperature −44.5 °C, mean annual accumulation rate 64 kg m^{-2} yr^{-1}, EPICA community members, 2006), two 1.2 m deep, 1.2 m wide and approximately 45 m long trenches in the firn, named T1 and T2, were excavated during the austral-summer field season 2012/2013 using a snow blower. Each trench was aligned perpendicularly to the local snow-dune direction. The horizontal distance between the starting points of T1 and T2 was 415 m.

To provide an absolute height reference, vertically aligned bamboo poles were stuck into the snow every 60 cm applying a spirit level. Additionally, a laser level device was

CPD
11, 5605–5649, 2015

used to check the bamboo pole heights, yielding in each snow trench a vertical accuracy better than 2 cm. No absolute height reference between the two trenches could be established, but, based on a stacked laser level measurement, the vertical difference between the trenches was estimated to be less than 20 cm.

Both trenches were sampled for stable-water-isotope analysis with a vertical resolution of 3 cm. In T1, 38 profiles were taken at variable horizontal spacings between 0.1 and ∼ 2.5 m. In T2, due to time constraints during the field campaign, only four profiles at positions of 0.3, 10, 30 and 40 m from the trench starting point were sampled. All firn samples (a total number of $N = 1507$) were stored in plastic bags and transported to Germany in frozen state. Stable isotope ratios were analysed using Cavity Ring-Down Spectrometers (L2120i and L2130i, Picarro Inc.) in the isotope laboratories of the Alfred Wegener Institute in Potsdam and Bremerhaven. The isotope ratios are reported in the usual delta notation in per mil (‰) as

$$\delta = \left(\frac{R_{\text{sample}}}{R_{\text{reference}}} - 1 \right) \times 10^3, \tag{1}$$

where R_{sample} is the isotopic ratio of the sample ($^{18}O/^{16}O$) and $R_{\text{reference}}$ that of a reference. The isotopic ratios are calibrated to the international V-SMOW/SLAP scale by means of a linear three-point regression analysis with different in-house standards. Additionally, a linear drift-correction scheme and a memory-correction scheme (adapted from van Geldern and Barth, 2012) is applied. The memory correction allows the reduction of repeated measurements per sample; here, we have used three repeated measurements instead of six suggested for Picarro instruments when no memory correction is applied, thereby approximately halving the measurement time. The analytical precision of the calibrated $\delta^{18}O$ measurements of all trench samples is on average 0.09 ‰.

CPD
11, 5605–5649, 2015

3 Results

3.1 Trench isotope records

The firn samples obtained from trench T1 provide a two-dimensional image of the $\delta^{18}O$ structure of the upper ~ 1 m of firn on a horizontal scale of ~ 50 m (Fig. 1a).

The surface height profile of the trench exhibits a snow topography which is typical for the sampling region. It is characterised by small-scale dunes with their main ridges elongated parallel to the mean wind direction, significantly higher density than the surrounding firn, and typical spatial dimensions of 4 m width, 8 m length and 20 cm maximum height (Birnbaum et al., 2010). Trench T1 features one prominent dune located between 25–40 m, accompanied by a dune valley between ~ 8–18 m, and some smaller-scale height variations. The peak-to-peak amplitude of the large dune undulation is ~ 10 cm, the entire height variations exhibit a standard deviation (SD) of 2.9 cm. The trench surface height profile is adopted as a local coordinate system (surface coordinates), the mean surface height serves as reference for absolute coordinates.

Overall, the trench $\delta^{18}O$ record shows a diverse picture. The delta values observed in T1 span a range from −54 to −34 ‰ with a mean of −44.4 ‰. A similar range of −50 to −38 ‰ is observed in T2 (Fig. 2) with a mean of −44.0 ‰. We can clearly identify alternating layers of high and low isotopic composition in the T1 record. Following the surface undulations, the uppermost layer (first 6 cm) shows high but also strongly variable $\delta^{18}O$ values between −54 and −34 ‰ with a variance of 19 $(‰)^2$, thereby already spanning the range of the entire trench record. Less negative values tend to be located in the valleys, however, the limited data do not allow to conclude whether this is a general feature. Located below this first layer, a band of generally lower $\delta^{18}O$ values is found in an absolute depth of 5–20 cm, likewise following the snow surface but exhibiting less horizontal variability with a range of −53 to −46 ‰.

To further analyse the layering, we track the pronounced maxima and minima of $\delta^{18}O$ values along the trench by automatically determining the local extrema of each isotope profile and visually assigning summer and winter to these extrema, resulting in lateral

CPD
11, 5605–5649, 2015

seasonal layer profiles as a function of depth (Fig. 1b). Implicitly this assumes that the past isotopic isolines are also temporal isolines which is a rough approximation considering the highly variable isotopic composition of the surface layer (Fig. 1a). Our results of the seasonal layer profiles will thus likely overestimate the respective surface height profile of each past season. To analyse the similarity between the past seasonal layer profiles and the present surface, we calculate the root-mean-square deviation (rmsd) between the vertical anomalies, i.e., the mean-subtracted seasonal layer profiles, and the horizontal reference as well as the present surface height profile. We find that the first summer layer follows the present surface undulations (rmsd difference of 1.8 cm between the comparison to the horizontal and the surface profile reference). The next three layers show on average a much weaker link with the present surface (rmsd difference of 0.5 cm), and the layers below 40 cm are on average horizontally aligned (difference of −0.8 cm). Comparably to the present surface undulations, the vertical layer anomalies feature peak-to-peak amplitudes of 6–24 cm (average SD of 3.7 cm). Supporting our above assumptions, the vertical separation of the observed lateral layer profiles is approximately 20 cm, in accord with the local mean annual accumulation rate of snow (64 kg m^{-2} yr^{-1}) and the mean firn density of ρ_{firn} = 340 kg m^{-3} measured in trench T1. The layering is strongly perturbed primarily in the depth of ∼ 60–100 cm for profile positions < 30 m. Here, a broad and diffuse region of rather constant δ^{18}O values around −40 ‰ is present together with a very prominent, 20 cm-thick feature of high delta values between 18 and 28 m.

The four profiles obtained from trench T2 (Fig. 2) show similar results as trench T1. Roughly five seasonal cycles can be identified, however, with remarkable inter-profile deviations especially at depths of 50–90 cm. This coincides with the region of strong perturbations identified in T1. As in trench T1, the T2 profiles suggest a direct relation between the isotopic layering and the local snow height profile for the surface snow, i.e., till a depth of 10–20 cm. Below that, the profiles diverge considerably (not shown) but show a better alignment on absolute coordinates (Fig. 2).

CPD
11, 5605–5649, 2015

3.2 Single-profile representativity

On the horizontal dimension of the trenches, the observed lateral variance (Fig. 3) reflects processes that are not related to variations of atmospheric temperatures as these are coherent on this spatial scale. According to the terminology adopted here, the lateral variance is non-climate noise. The link between the lateral seasonal layer profiles of the isotopic composition and the present snow surface decreases with depth (Fig. 1b). This has direct consequences for the analysis of the lateral variability of δ^{18}O values (Fig. 3). For the first 20 cm, the lateral variance is significantly higher when evaluated on absolute coordinates than on surface coordinates (mean of 16.0 $(‰)^2$ vs. 7.8 $(‰)^2$, $p = 0.1$). For older firn layers ($z < 20$ cm) the situation seems to reverse with a mean of 3.6 $(‰)^2$ in the former and 4.5 $(‰)^2$ in the latter case. In both cases, the lateral variance shows a pronounced drop from high values in the surface layer to rather constant values deeper in the firn. The overall mean lateral variability of the T1 record is $\sigma^2_{l,T1} \simeq 5.9\,(‰)^2$. Due to the rather horizontal stratigraphy of the isotopic composition in the deeper trench parts all further plots and calculations will refer to the horizontal reference and not to the actual snow surface.

The observation of such a considerable lateral variance or noise level poses the questions on how representative single firn profiles from low-accumulation sites are, and how much they reflect the original climate signal that is sought to be reconstructed. One indicator for the similarity of profiles is the pairwise Pearson correlation coefficient. The possible correlations ($N = 152$) between single profiles of T1 and single profiles of T2 (Fig. 4) are substantially scattered around a mean of ~ 0.50 (1 SD = 0.13). Each single correlation mimics the potential result obtained from correlating two "classical" snow pits taken at a distance of 500 m. Due to the lack of an absolute height reference between the trenches, vertical shifting of the T2 profiles of up to ±12 cm is allowed to maximise the correlations. The relative majority (~ 43 %) of the profile pairs shows an optimal shift of +3 cm which is well below the estimated upper vertical height difference of the trenches. Our results indicate that only by chance the classical snow-pit

CPD
11, 5605–5649, 2015

method can yield two profiles that share significant common features (half of the profile pairs show a correlation ≤ 0.49, only two pairs ($\sim 1.3\,\%$) exhibit a correlation above 0.8). In general, due to the inherent noise, single firn profiles cannot be regarded as representative recorders of isotopic proxy signals on the vertical scales analysed here.

3.3 Spatial noise structure

To quantify the spatial noise structure in the trench isotope record, we investigate the inter-profile correlation as a function of profile spacing (Fig. 5). To this end, all possible profile pairs for a given spacing are selected, allowing a tolerance in the lateral position of 5 %, and the mean inter-profile correlation of the pairs is calculated. The correlation approaches one for nearest neighbours and rapidly drops with increasing inter-profile distance before it stabilises around a value of ~ 0.5 for spacings $\gtrsim 10\,\mathrm{m}$.

This spatial correlation structure can be described using a simple statistical model: We assume that each profile consists of a common signal S and a noise component ε independent of the signal. The noise component is modeled as a first-order autoregressive process (AR(1)) in the lateral direction. The inter-profile correlation coefficient can then be expressed (see Appendix A) as

$$r_{XY} = \frac{1}{1 + \frac{\mathrm{var}(\varepsilon)}{\mathrm{var}(S)}} \left\{ 1 + \frac{\mathrm{var}(\varepsilon)}{\mathrm{var}(S)} \exp\left(-\frac{|x-y|}{\lambda} \right) \right\} . \tag{2}$$

Here, $\mathrm{var}(\varepsilon)/\mathrm{var}(S) =: F^{-1}$ is the inverse of the signal-to-noise variance ratio of the profiles, $|x-y|$ is the inter-profile spacing, and λ denotes the decorrelation length of the autocorrelation. The variance ratio determines the limit of Eq. (2) for $|x-y| \to \infty$. It is estimated from the data using the mean inter-profile correlation for the profile spacings between 10–35 m, giving a value of $F^{-1} = 1.1 \pm 0.1$. An estimate of the decorrelation length is obtained from the lateral $\delta^{18}\mathrm{O}$ variations of T1 by calculating the autocorrelation at a lag of $\Delta\ell = 1\,\mathrm{m}$. To account for the irregular lateral sampling, we apply the

CPD
11, 5605–5649, 2015

Gaussian kernel correlation discussed in Rehfeld et al. (2011) and find that the noise correlation has decreased to $1/e$ at a distance of $\lambda \simeq 1.5\,\mathrm{m}$.

The signal-to-noise variance ratio can also be directly estimated from the data if we identify the noise variance with the mean lateral trench variance, $\mathrm{var}(\varepsilon) = \sigma_{\mathrm{l}}^2$, and assume that the noise is isotropic and independent of the signal. Then, the signal variance $\mathrm{var}(S)$ can be estimated with the mean down-core variance σ_{v}^2 (T1: $\sigma_{\mathrm{v,T1}}^2 \simeq 9.5\,(‰)^2$, T2: $\sigma_{\mathrm{v,T2}}^2 \simeq 7.3\,(‰)^2$) reduced by the noise variance. For T1 we obtain $\mathrm{var}(S) \simeq \sigma_{\mathrm{v,T1}}^2 - \sigma_{\mathrm{l,T1}}^2 = 3.6\,(‰)^2$. This gives a variance ratio of ~ 1.6 which is of the same order of magnitude as the estimate from the inter-profile correlation but slightly underestimates the signal strength.

3.4 Trench mean profiles

The spatial mean of all T1 profiles (Fig. 6) is highly correlated with the spatial mean of the T2 profiles ($r_{\mathrm{T1,T2}} = 0.81$), indicating a common seasonal isotopic signal reproducible over a spatial scale of at least 500 m. It is interesting to note that this value is above most of the single inter-profile correlations (Fig. 4). Due to the surface undulations, the number of existing observations evaluated on absolute coordinates varies for the first three depth bins. To obtain non-biased mean profiles, only the depth range covered by all profiles is used in the averaging process. A vertical shift of the mean T2 profile of ±12 cm was allowed to maximise the correlation and, consistent to the results obtained for single profiles, an optimal shift of +3 cm was obtained. In both profiles, we observe five seasonal cycles spanning a range of ~ 6–7 ‰ at the surface, but being attenuated further down and exhibiting no clear sinusoidal shape in the "fourth" year (65–90 cm depth). Interestingly, this obscured part without any clear signal of depleted $\delta^{18}\mathrm{O}$ "winter" values is found in both trenches, indicating that this feature persists over several hundred of metres and is thus likely of climatic origin. Despite the statistically significant correlation ($p = 0.01$, accounting for the full autocorrelation structure and allowing for vertical shifting of ±12 cm), pronounced differences between the mean

CPD
11, 5605–5649, 2015

profiles are present, such as a significantly lower isotopic composition of the T2 mean between 50–80 cm and a considerably higher one within depths up to ∼ 40 cm as well as for the lowermost region of the trenches.

In order to obtain annual-mean δ^{18}O time series we define annual bins through the six local maxima determined from the averaged profile of the two mean trench profiles. The mean peak-to-peak distance of these maxima is 19.8 cm, consistent with the accumulation rate. Three alternative sets of annual bins are derived from the five local minima as well as from the midpoints of the slopes flanking these minima. The annual-mean time series derived from these four sets are averaged to obtain a single time series for each trench (Fig. 6). The correlation of the average annual-mean δ^{18}O time series of $0.87^{+0.07}_{-0.20}$ (range represents the four binning methods) is comparable to that of the mean seasonal profiles (0.81). However, five observations of annual means are too short to reliably estimate the correlation and its significance.

4 Discussion

Climate reconstructions based on proxy data rely on the assumption that at least part of the measured signal is related to a climate parameter, such as temperature in case of ice/firn-core derived δ^{18}O (Dansgaard, 1964). However, proxy signals are inherently noisy with uncertainties arising prior to deposition of the proxy into the archive, post-depositionally during archive storage, as well as later in the human sampling and measurement process (Evans et al., 2013; Laepple and Huybers, 2013; Steig, 2009).

Our trench data confirm earlier results that individual firn records of δ^{18}O from low-accumulation regions are strongly influenced by local noise (Fisher et al., 1985; Karlöf et al., 2006). However, going beyond this finding, our two-dimensional δ^{18}O dataset also allows to determine the spatial structure and to learn about the causes of the noise. In this section, we discuss our findings in the context of the possible noise sources and derive implications for inter-annual climate reconstructions based on firn cores.

CPD
11, 5605–5649, 2015

4.1 Trench δ^{18}O variance levels

A hypothetical, horizontally stratified trench with zero isotopic variance in lateral direction would yield perfectly correlated single profiles. However, in the actual trenches we observe a high lateral variance (see Fig. 3 for T1) with a mean variance that is comparable to the mean down-core variance (Table 1).

Several pre- and post-depositional effects induce lateral variance of the firn layer, the relative importance of each varies on the spatial scales considered. Starting on the m-scale, the principal contribution is induced by the surface roughness, closely related to snow drift events including spatial redistribution, erosion, reworking and dune formation ("stratigraphic noise", Fisher et al., 1985). Possibly, exchange of water vapour with the atmosphere by sublimation-condensation processes (Steen-Larsen et al., 2014), potentially accompanied by forced ventilation (Waddington et al., 2002; Neumann and Waddington, 2004; Town et al., 2008), acts as a further noise source. Going to larger spatial scales ($\gtrsim$1 km), spatial precipitation intermittency (e.g., Richardson et al., 1997; Persson et al., 2011; Sime et al., 2009, 2011) presents an additional component, influencing a certain snow layer via spatially varying precipitation weighting.

The down-core variance includes the isotopic signal from seasonal and longer climate variations. In addition, the vertical isotope record is also subject to modifications arising prior to and after the deposition of snow. Temporal precipitation intermittency can bias the δ^{18}O record (Laepple et al., 2011) but also induces vertical variability caused by inter-annual variations of the timing of precipitation events (Persson et al., 2011; Sime et al., 2009, 2011). Diffusion of water vapour through the porous firn along seasonal isotopic gradients (Johnsen, 1977; Johnsen et al., 2000; Whillans and Grootes, 1985; Cuffey and Steig, 1998) obscures seasonal and longer isotopic cycles, depending on the accumulation rate. Forced ventilation acts perpendicular to the pressure isolines in the firn, generated by the steady wind flow across the undulating surface (Waddington et al., 2002). Depending on the dune undulations, this may en-

CPD
11, 5605–5649, 2015

hance the vertical diffusion in the first tens of centimetres of firn and shorten the time for the snowpack to reach isotopic equilibration.

The pronounced drop in the lateral variance with depth (Fig. 3) can likely be explained by isotopic diffusion. This is suggested by a simple numerical estimate diffusing an artificial trench record that initially exhibits a rectangular isotope variation (25 % summer precipitation) as well as a sinusoidal surface topography with a wavelength of 10 m and a peak-to-peak amplitude of 10 cm (Fig. B1, see Appendix B for details). While these are promising results, the theoretical estimate of Waddington et al. (2002) as well as a numerical diffusion model including forced ventilation by Neumann and Waddington (2004) showed that the true rate of diffusion in the first metre might be higher. Furthermore, Town et al. (2008) demonstrated that forced ventilation also attenuates the seasonal cycle. In total, at the current stage of investigation we are not able to clarify the importance of water vapour exchange and forced ventilation. For this, more field measurements and a thorough numerical treatment are necessary.

4.2 Spatial structure of lateral variance

In Sect. 3.3 we showed that the inter-profile correlation as a function of profile spacing (Fig. 5) can be described by a common signal overlayed by lateral noise following an AR(1) model.

This demonstrates firstly that each single trench profile features a local isotopic signal common only over a few metres which is induced by small-scale covarying noise. The decorrelation length of ~ 1.5 m of this noise is related to the intermittent deposition of snow and, in particular, to the dune scale: A sinusoidal surface height variation with a wavelength ν of $\lesssim$10 m would lead to zero autocorrelation for a shift of $\nu/4$, similar to our observations. While the real surface topography is more complicated, it suggests that stratigraphic noise is an important noise component in our δ^{18}O records. In addition, vapour exchange with the atmosphere driven by forced ventilation might contribute to the overall noise level since it is likewise related to the surface roughness. Secondly, the remaining correlation of ~ 0.5 for inter-profile spacings of $\gtrsim$10 m, implying roughly

CPD
11, 5605–5649, 2015

the same amount of signal and noise variance in single profiles, is due to a regionally coherent ($\lesssim$1 km) isotope signal, supported by the fact that it is comparable to the mean correlation between individual T1–T2 records (Fig. 4). However, this regional isotope signal does not directly translate into a regional climatic signal of local surface air temperature as various effects can influence the isotopic composition of precipitation (Jouzel et al., 1997). Further, there is the possibility of an additional noise component with a spatial decorrelation length larger than the distance between both trenches, for example caused by spatial precipitation intermittency.

The spatial autocorrelation structure and the inter-profile correlation provide estimates of an optimal sampling strategy for firn-coring efforts in the study region. To ensure that the local noise is uncorrelated, single profiles should be spaced at distances several times the decorrelation length. Visually, we find a minimum spacing of $\sim$ 10 m to be optimal (Fig. 5).

4.3 Representativity of isotope signals on seasonal to inter-annual time scales

Our statistical model of covarying stratigraphic noise allows to determine the seasonal signal content depending on the number of profiles and the profile spacing. As the model is entirely based on parameters estimated from the T1 data, we can use the T2 data to validate the model. Therefore, we determine and predict the correlation of an averaged set of T1 profiles with the T2 trench mean, the latter thus serving as a reference isotopic signal.

To determine the correlation from the data for a given number of profiles and a profile spacing, all possible unique sets of T1 profiles are selected that fulfill the given criteria. Due to the uneven spacing of the T1 profiles, we allow an absolute uncertainty of the spacing between the profiles in a set of 0.5 m. The correlation is given as the mean correlation over all sets. Empirically, we find a steady increase in the correlation with the T2 reference for increasing number of profiles used in the T1 set (Fig. 7). The observed increase in correlation is expected since also for autocorrelated noise the noise variance of the set decreases with the number of profiles. Additionally, as a direct

CPD
11, 5605–5649, 2015

consequence of the autocorrelation structure, the correlation increases with a wider spacing between the individual profiles of the T1 set (Fig. 7). A given number of profiles at a spacing of 2.4 m share more common noise variance than the same number of profiles at a larger spacing. Thus, when the two profile sets are averaged, the latter set will show a higher correlation with the reference signal. This finding also explains the comparable reduction of the noise levels of the trench mean profiles (for T1 the levels drop by 46 % compared to the mean of the individual down-core variances, for T2 by 55 % (Table 1)): The 38 T1 profiles have varying inter-profile distances from 0.1–2.5 m, whereas the four T2 profiles are already spaced at large, more optimal distances of 10–20 m.

Our noise model allows to calculate the theoretical inter-trench correlation coefficient (Eq. A13). Using the variance ratio of $F^{-1} = 1.1$ obtained in Sect. 3.3, the model prediction is in good agreement with the empirical data (Fig. 7). We can conclude that the first-order autoregressive noise model captures the major noise component for isotopic records on spatial scales of at least 500 m as well as on temporal scales of a few years.

With the noise model validated between the trenches, implications for climate reconstructions using firn-core isotope records can be deduced. We define the representativity of a set of trench profiles as the correlation of this set with a hypothetical, common climate signal (Eq. A12). This representativity can be interpreted as the upper limit of the correlation to a temperature times series obtained from a weather station located in the study region. In the limit of independent noise terms (vanishing autocorrelation), our definition of representativity yields the same expression as derived by Wigley et al. (1984).

The representativity is time-scale-dependent since signal and noise variance are both a function of the time scale. For example, the seasonal variability is much larger than any year-to-year variations of the istopic signal. Analysing seasonal variability, the representativity can be readily calculated with the variance ratio F^{-1} given above. For reconstructions on inter-annual time scales, the isotope records are additionally averaged in the vertical direction and thus, the results depend on the vertical noise

CPD
11, 5605–5649, 2015

covariance. Snow-pit studies around Vostok station have shown significant temporal non-climatic oscillations of the isotopic composition (Ekaykin et al., 2002), indicating a vertical spatial noise structure. The observed time scales of the oscillations range from 10^0–10^1, possibly up to 10^2 years, and are linked to the movement of accumulation waves of various scales. Here, due to the limited data coverage in vertical direction, we are only able to investigate two limiting cases. As the simplest best-case scenario (case I), the vertical noise covariance is given by an AR(1) process as in the lateral direction. In the worst case (case II), averaging one annual firn layer does not reduce the noise level at all, assuming a complete interdependence of the noise on the sub-annual time scale. The variance ratio of noise over signal is for the inter-annual time scale thus given by

$$F^{-1}_{\text{annual}} = \frac{\text{var}(\varepsilon)_{\text{annual}}}{\text{var}(S)_{\text{annual}}} = \begin{cases} \frac{\text{var}(\varepsilon)\sigma^{*2}_{\text{annual}}}{\text{var}(S)_{\text{annual}}} & \text{case I} \\ \frac{\text{var}(\varepsilon)}{\text{var}(S)_{\text{annual}}} & \text{case II.} \end{cases} \quad (3)$$

The effective annual noise variance $\text{var}(\varepsilon)\sigma^{*2}_{\text{annual}}$ (Eq. A11) for case I depends on the autocorrelation parameter a_{annual} which is estimated from the mean autocorrelation function of the vertical δ^{18}O data of T1 after subtracting the mean seasonal profile. We obtain a value of $a_{\text{annual}} \approx 0.61$ for a lag of $\Delta\ell = 3$ cm, equivalent to a decorrelation length of $\lambda_{\text{annual}} \approx 6$ cm. As the best-possible estimate, an annual signal variance of $\text{var}(S)_{\text{annual}} \simeq 0.68\,(‰)^2$ is obtained from the mean of the variances of the annual δ^{18}O time series (Fig. 6) of the two trenches (Table 1). The seasonal noise variance $\text{var}(\varepsilon)$ is set to the observed mean lateral T1 variance (Table 1). Altogether, we obtain an annual variance ratio of $F^{-1}_{\text{annual}} \simeq 1.8$ for case I, and of $F^{-1}_{\text{annual}} \simeq 8.7$ for case II. Note that using the seasonal noise variance as calculated from the entire trench data might represent a slight overestimation given the exceptionally high variability observed in the surface layer (Fig. 3).

For single profiles, the representativity on the seasonal time scale is around 0.69 (Fig. 8). On the inter-annual time scale, single profiles have a representativity of 0.59

CPD
11, 5605–5649, 2015

in the best-case scenario (Fig. 8a) and a much lower one in the worst-case scenario (0.32, Fig. 8b).

In general, the representativity increases with the number of profiles averaged, and the increase is stronger for larger inter-profile spacings. However, spacings above 10 m do not increase the representavities any further as the stratigraphic noise is practically decorrelated (Fig. 5). To obtain a representativity of 0.8 for inter-annual signals with profiles separated by 10 m, one needs to take a minimum of 4–16 cores (from best to worst case). Demanding a representativity of 0.9, the number of cores required increases to 8–37.

The low single-profile representativity on the inter-annual time scale is consistent with previous findings from Dronning Maud Land. The 16 annually resolved $\delta^{18}O$ records of the study of Graf et al. (2002), taken in an area extending 500 km from east to west and 200 km from north to south, showed a low signal-to-noise variance ratio in the individual records of $F = 0.14$. Due to the large inter-profile spacing, the stratigraphic noise covariance in the records is decorrelated. Then, the variance ratio F from the cross-correlations directly translates into the representativity of a single profile as $r_{SX} = 1/\sqrt{1 + F^{-1}} \simeq 0.35$, consistent with our findings for the worst-case scenario (case II). However, this accordance does not necessarily mean that our worst-case scenario is the more realistic one since the measured cross-correlations are also subject to potential dating uncertainties and additional variability caused by spatially varying precipitation-weighting and possibly other effects.

Stratigraphic noise does not only affect isotopic records but also other proxies derived from ice cores, such as aerosol-derived chemical constituents. Gfeller et al. (2014) investigated the representativity of ion records from five Greenland firn cores on seasonal and inter-annual time scales, taken at varying distances from 7–10 m in the vicinity of the NEEM drilling site. With the definition of representativity based on the theoretical work of Wigley et al. (1984), for inter-annual time scales Gfeller et al. (2014) found representativities of ~ 0.55–0.84 for single cores, and of ~ 0.84–0.95 for the average of all five cores, depending on the ions considered. These numbers are

CPD
11, 5605–5649, 2015

slightly higher than our best-case-scenario results for $\delta^{18}O$, a fact which is expected as the accumulation rate at the NEEM site is about three times higher than at Kohnen station (NEEM community members, 2013).

4.4 Implications

The noise level identified in our trench data poses a significant challenge for the interpretation of firn-core-based climate reconstructions on seasonal to inter-annual time scales. In the following, we discuss examples of implications of the noise model concerning (1) the required measurement precision of water isotopes, (2) the potential noise fraction in isotope signals of the EDML ice core and (3) the detectability of anthropogenic temperature trends in low-accumulation firn cores.

The noise of an isotopic signal consists of the stratigraphic noise discussed here as well as the noise caused by the measurement process. Thus, obtaining the best signal is a trade-off between measurement precision and the amount of analysed samples.

For seasonal as well as on inter-annual time scales, the measurement uncertainty of the trench data of $\Delta\delta^{18}O = 0.09‰$ is much lower ($\sim$ 4–8 %) than the standard deviation of the stratigraphic noise (Table 2). This ratio is independent of the temporal resolution if a lower temporal resolution is obtained by averaging annually resolved data as both, the noise level and the measurement uncertainty, decrease by the same amount in the averaging process, assuming independence between the samples. In such a case, priority should be given to measuring and averaging across multiple cores in order to reduce the (stratigraphic) noise levels instead of performing high-accuracy measurements on single cores, given that we are only interested in $\delta^{18}O$. As an example, for Cavity Ring-Down Spectrometers as those that have been used for this work, much faster measurements are possible by reducing the number of repeated measurements down to one per sample, resulting only in a slight decrease in measurement precision when a memory correction scheme as applied to our data is used.

CPD
11, 5605–5649, 2015

If a lower temporal resolution is obtained by a coarser sampling of firn cores, the measurement error to stratigraphic noise ratio will depend on the analysed resolution (Table 2). For a resolution corresponding to ten years, our measurement uncertainty might amount to up to 25 % of the stratigraphic noise level, assuming independence of the stratigraphic noise between the years. For our data, the noise level of single cores would become comparable to the measurement uncertainty for averages over ∼ 154 years (case I) or ∼ 728 years (case II).

The deep EPICA Dronning Maud Land ice core obtained in the vicinity of Kohnen station shows the climate evolution in Antarctica over the last 150 000 years (EPICA community members, 2006). Oerter et al. (2004) studied a section of the core covering the last 6000 years with a resolution of ten years (their Fig. 2). We find a decadal variance for this part of the core of $\sim 0.57\,(‰)^2$. If we assume that our estimates of the stratigraphic noise variance hold over the last couple of thousand years, then ∼ 20–100 % of the decadal variance seen in the EDML core over this time period might be simply noise (Table 2). In order to reconstruct the Holocene climate variability of the last millennium from low-accumulation regions, there is thus the clear need to either average across multiple cores based on the results of the previous section, or, if only the magnitude of variability is of interest, to correct the proxy variability for the noise contribution (e.g., Laepple and Huybers, 2013).

As a final example of applying our noise model, we estimate the ability of firn cores close to the Kohnen station to reconstruct a potential warming trend of the last decades. In the last 50 years, the surface temperature over East Antarctica has warmed by about half a degree (Steig et al., 2009). The probability to detect this trend or to reconstruct its slope is estimated using a Monte Carlo approach creating 10^5 δ^{18}O time series consisting of a signal (the linear temperature trend) and uncorrelated Gaussian noise with variance equal to the annual trench noise variance for the best as well as the worst case (Table 2). The trend is detected when the correlation of the time series with the signal is positive at the significance level of $p = 0.05$. We define the probability for determining the right slope as the fraction of cases where a linear regression yields

CPD
11, 5605–5649, 2015

a slope that lies in a range of 25 % around the true slope. To simplify matters, we assume a temperature-to-isotope gradient for $\delta^{18}O$ of 1 ‰ K^{-1}, given the considerable uncertainties associated with the spatial and temporal gradients discussed in the literature (e.g., Jouzel et al., 1997). We note that in general the $\delta^{18}O$ slope very likely lies below 1 ‰ K^{-1} (~ 0.8 ‰ K^{-1} for DML, EPICA community members, 2006) which implies yet lower detection probabilities since the signal variance is then even smaller compared to the noise variance. Finally, in the case of multiple cores it is assumed that they are taken at distances on which the autocorrelation of the stratigraphic noise is decorrelated (≥ 10 m).

The probability to detect the trend or to reconstruct its slope is below 20 % for single cores (Fig. 9). To reliably (> 80 % of the cases) detect the warming over the East Antarctic plateau, our results suggest that averaging across at least $\sim$ 10–50 firn cores taken at spacings of 10 m (Fig. 9) is needed, depending on the scenario for the annual noise variance. Inferring the right slope would need three times that number of cores.

5 Conclusions

We presented extensive oxygen stable water isotope data derived from two snow trenches excavated at Kohnen station in Dronning Maud Land, Antarctica. The two-dimensional approach allowed a thorough investigation of the representativity of single firn-core isotope profiles, as well as of the spatial structure of the signal and noise over spatial scales of up to 500 m and a time span of approximately five years.

The trench data confirm previous studies that single isotope profiles obtained from low-accumulation regions are poorly correlated and do not show a coherent signal, but also demonstrated that the spatial average of a sufficient number of profiles provides a representative isotopic signal. We further show that single profiles are strongly influenced by local, small-scale noise that exhibits a spatial covariance. A statistical model describing this noise as a first-order autoregressive process successfully explains the observed covariance structure and allows to reproduce the observed correlation statis-

CPD
11, 5605–5649, 2015

tics between the trenches. The autocorrelation of the noise occurs on spatial scales that are of the same order of magnitude as the surface height variations introduced by sastrugi and dunes and the intermittent deposition of snow, suggesting stratigraphic noise as a major noise source. Extending the ordinary stacking of isotope records, our results are used to infer appropriate sampling strategies. We derive the representativity of isotope profiles for seasonal to annual resolution depending on the number of firn cores and the inter-core spacing. For our low-accumulation (64 mm w.eq. yr^{-1}) study region, we find an optimal profile spacing of about 10 m where the noise covariance is sufficiently decorrelated. The representativity depends on the time scale: For seasonal resolution, five profiles taken with the optimal spacing are sufficient to obtain representative ($R > 0.9$) isotope signals; on inter-annual time scales, $\sim$ 2–8 times as many profiles would be needed.

The low representativity of single firn profiles at our site hampers the quantitative interpretation of isotope in terms of climate variations. The noise level observed in the trench data suggests that large parts of the decadal variations seen in the EPICA DML ice core over the last 6000 years might be noise. In addition, we show that faithfully reconstructing the recent positive temperature trend observed over the East Antarctic plateau is impossible by drilling only single cores; instead, averaging at least 10–50 firn cores would be necessary. This task is rendered easier by the fact that the annual noise level is substantially larger than typical measurement uncertainties. Therefore, for high-resolution single-proxy reconstructions it might be more advantageous to conduct less precise measurements, e.g., by operating Cavity Ring-Down Spectrometers with only one injection per sample, for the benefit of analysing many cores.

Since the stratigraphic noise is related to the intermittent deposition of snow and the formation of surface dunes, it depends primarily on the local accumulation rates, besides further factors such as wind strength, temperature, seasonal timing of the precipitation and snow properties. Therefore, to a first approximation we expect that our representativity results improve (worsen) for regions with higher (lower) accumulation rates. In effect, results similar to ours likely hold for large parts of the East Antarctic

CPD
11, 5605–5649, 2015

plateau, but trench-like approaches in West Antarctica and Greenland – regions with considerably higher accumulation rates – are needed. In addition, studies with deeper trenches that cover longer times of isotopic variations are necessary to enhance our knowledge about the vertical noise covariance structure which is crucial to determine the representativity on longer time scales. Deeper trenches would also allow to link our representativity results to actual correlations with temperature time series derived from weather stations. The latter is part of ongoing work at Kohnen station.

Appendix A: Derivation of noise model

The Pearson pairwise correlation coefficient of two time series, or profiles, X and Y reads

$$r_{XY} = \frac{\mathrm{cov}(X,Y)}{\sigma_X \sigma_Y}, \tag{A1}$$

where σ_X and σ_Y are the standard deviations of profile X and profile Y, respectively, and $\mathrm{cov}(X,Y)$ is the covariance of the profiles given by

$$\mathrm{cov}(X,Y) = \langle XY \rangle - \langle X \rangle \langle Y \rangle . \tag{A2}$$

Here, $\langle \cdot \rangle$ denotes the temporal average, thus the spatial average in vertical direction for a trench profile.

We now assume that a trench isotope profile $X_n(t)$ consists of a signal part $S(t)$ and a noise component $\widetilde{\varepsilon_n}(t)$ that is independent from the signal and following a standard normal distribution. In addition, to account for the spatial covariance of the noise in lateral direction, we assume each noise term to be following an AR(1) autoregressive proccess,

$$X_n(t) = S(t) + \widetilde{\varepsilon_n}(t)$$

CPD
11, 5605–5649, 2015

$$= S(t) + a\widetilde{\varepsilon_{n-1}}(t) + \sqrt{1-a^2}\varepsilon_n(t)\,. \tag{A3}$$

Here, a is the autocorrelation parameter with $0 \le a \le 1$, and the square-root term in front of $\varepsilon_n(t)$ is a normalisation. If we consider P equidistant trench profiles numbered $1, 2, \ldots, P$, the noise term of profile n can be given recursively,

$$X_n(t) = S(t) + a^{n-1}\varepsilon_1(t) + \sqrt{1-a^2}\sum_{i=2}^{n} a^{n-i}\varepsilon_i(t)\,. \tag{A4}$$

With the help of Eq. (A4), we can calculate the spatial mean of a set of N trench profiles,

$$\begin{aligned}
\overline{X}(t) :=& \overline{\left\{X_{n_1}(t), X_{n_2}(t), \ldots, X_{n_N}(t)\right\}} \\
=& S(t) + \frac{1}{N}\left\{\left(\sum_{i=n_1}^{n_N} a^{i-1}\right)\varepsilon_1(t)\right. \\
&\left. + \sqrt{1-a^2}\left(\sum_{i=2}^{n_1} a^{n_1-i}\varepsilon_i(t) + \cdots + \sum_{j=2}^{n_N} a^{n_N-j}\varepsilon_j(t)\right)\right\} \\
=& S(t) + \frac{1}{N}\left\{\left(\sum_{\nu} a^{\nu-1}\right)\varepsilon_1(t) + \sqrt{1-a^2}\sum_{i=2}^{\nu^*}\left(\sum_{k\in\{\nu>1,\,\nu\ge i\}} a^{k-i}\right)\varepsilon_i(t)\right\}
\end{aligned} \tag{A5}$$

where we have defined $\nu := \{n_1, n_2, \ldots, n_N\}$ and $\nu^* := \max(\nu)$.

From Eq. (A1) the inter-profile correlation coefficient can be calculated for general kinds of covarying noise terms, $\mathrm{cov}(\varepsilon_X, \varepsilon_Y) \neq 0$. With $\mathrm{cov}(X, Y) = \mathrm{var}(S) + \mathrm{cov}(\varepsilon_X, \varepsilon_Y)$, $\mathrm{var}(\varepsilon_X) = \mathrm{var}(\varepsilon_Y) \equiv \mathrm{var}(\varepsilon)$ and therefore $\mathrm{var}(X) = \mathrm{var}(S) + \mathrm{var}(\varepsilon_X) \equiv \mathrm{var}(Y)$ we obtain

$$r_{XY} = \frac{\mathrm{var}(S) + \mathrm{cov}(\varepsilon_X, \varepsilon_Y)}{\mathrm{var}(S) + \mathrm{var}(\varepsilon)}\,. \tag{A6}$$

CPD
11, 5605–5649, 2015

Further, the idendity $\mathrm{cov}(\varepsilon_X, \varepsilon_Y) = \langle \varepsilon_X \varepsilon_Y \rangle$, holds for noise. Thus, for AR(1)-autocorrelated noise (Eq. A4) the covariance reads

$$\mathrm{cov}(\varepsilon_X, \varepsilon_Y) = a^{\xi} \mathrm{var}(\varepsilon) \,\text{with}\, \xi := \frac{|x-y|}{\Delta\ell}. \tag{A7}$$

Here, $|x-y|$ is the distance between profile X and Y, and $\Delta\ell$ ist the spacing of adjacent profiles. This can be seen if we set, without loss of generality, $X = X_1$ and $Y = X_n$ and calculate the spatial mean $\left\langle \varepsilon_{X_1} \varepsilon_{X_n} \right\rangle$, noting that only products of identical noise terms have non-vanishing covariance. The parameter a is the value of the autocorrelation function at lag one, $a = \exp\left(-\Delta\ell/\lambda\right)$, where λ is the typical length scale on which the autocorrelation decreases to the value of $1/\mathrm{e}$. Thus, the covariance of the noise terms decreases exponentially with increasing inter-profile spacing $|x-y|$.

To obtain the representativity of a trench profile set, we correlate the profile set with the signal $S(t)$,

$$r_{S\overline{X}} = \frac{\mathrm{cov}(S, \overline{X})}{\sigma_S \sigma_{\overline{X}}}; \tag{A8}$$

correlating two profile sets yields the amount of variance shared by the sets,

$$r_{\overline{X}\overline{Y}} = \frac{\mathrm{cov}(\overline{X}, \overline{Y})}{\sigma_{\overline{X}} \sigma_{\overline{Y}}}. \tag{A9}$$

For statistically independent signal and noise terms we have $\mathrm{cov}(S, \overline{X}) = \mathrm{var}(S)$. For $\mathrm{cov}(\overline{X}, \overline{Y})$ we assume that one profile set is derived from T1, the other from T2. As the trenches are separated by $\sim 500\,\mathrm{m}$, the noise terms are to a good approximation decorrelated, and therefore $\mathrm{cov}(\overline{X}, \overline{Y}) \simeq \mathrm{var}(S)$. What is left to calculate is the variance $\sigma^2_{\overline{X}}$ of a profile set. A straightforward calculation, again noting that only products of

CPD
11, 5605–5649, 2015

identical noise terms do not vanish in the averaging process, yields

$$\sigma^2_{\overline{X}} = \langle \overline{X}^2 \rangle - \langle \overline{X} \rangle^2 = \langle \overline{X}^2 \rangle - \langle S \rangle^2$$
$$= \mathrm{var}(S) + \mathrm{var}(\varepsilon) \frac{\sigma^{*\,2}_{\overline{X}}}{N^2}. \tag{A10}$$

Here, $\mathrm{var}(\varepsilon)\sigma^{*\,2}_{\overline{X}}$ is the effective noise variance of the profile set using the definition

$$\sigma^{*\,2}_{\overline{X}} := \left(\sum_{\nu} a^{\nu-1} \right)^2 + (1-a^2) \sum_{i=2}^{\nu^*} \left(\sum_{k \in \{\nu > 1, \nu \geq i\}} a^{k-i} \right)^2. \tag{A11}$$

By combining Eqs. (A8) and (A9) with Eq. (A10), respectively, we finally obtain expressions for the representativity of a trench profile set as well as for the shared variance of a T1 and a T2 profile set:

$$r_{S\overline{X}} = \frac{1}{\sqrt{1 + \frac{\mathrm{var}(\varepsilon)}{\mathrm{var}(S)} \frac{\sigma^{*\,2}_{\overline{X}}}{N^2}}}; \tag{A12}$$

$$r_{\overline{XY}} \simeq \frac{1}{\left\{ \left(1 + \frac{\mathrm{var}(\varepsilon)}{\mathrm{var}(S)} \frac{\sigma^{*\,2}_{\overline{X}}}{N^2_{\overline{X}}} \right) \left(1 + \frac{\mathrm{var}(\varepsilon)}{\mathrm{var}(S)} \frac{\sigma^{*\,2}_{\overline{Y}}}{N^2_{\overline{Y}}} \right) \right\}^{1/2}}. \tag{A13}$$

For vanishing autocorrelation, $a \to 0$, Eq. (A11) gives $\sigma^{*\,2}_{\overline{X}} \to N$. Thus, the representativity of a profile set, Eq. (A12), simplifies to the classical result

$$r_{S\overline{X}} \xrightarrow{a \to 0} \frac{1}{\sqrt{1 + \frac{1}{N} \frac{\mathrm{var}(\varepsilon)}{\mathrm{var}(S)}}}, \tag{A14}$$

CPD
11, 5605–5649, 2015

where the noise variance scales with the number of profiles averaged.

For the full trench data, Eqs. (A12)–(A13) are referred to as the representativities on the seasonal time scale with the corresponding seasonal variance ratio of $\frac{\mathrm{var}(\varepsilon)}{\mathrm{var}(S)}$. On the inter-annual time scale, this variance ratio is replaced by the corresponding annual ratio of $\frac{\mathrm{var}(\varepsilon)_{\mathrm{annual}}}{\mathrm{var}(S)_{\mathrm{annual}}}$, where for the annual noise variance, $\mathrm{var}(\varepsilon)_{\mathrm{annual}}$, the two limiting cases discussed in the text are used.

Appendix B: Estimate of the influence of isotopic diffusion

To estimate the effect of isotopic diffusion through the porous firn on the lateral δ^{18}O variance of the trenches, we apply a simple numerical approach. An artificial δ^{18}O trench of 45 m length and 1.2 m depth is built by creating isotope profiles with a rectangular δ^{18}O variation (expressed as relative variation between −1 and 1) adopting a summer fraction of 25 %. The lateral resolution is set to 0.6 m, resulting in 76 profiles; the vertical resolution is fixed at 0.5 cm. Each profile is vertically shifted to mimic a surface height variation d of the form

$$d(x) = \Delta \cdot \sin\left(\frac{2\pi}{\lambda} x\right) \tag{B1}$$

with a peak-to-peak amplitude of $2\Delta = 10$ cm and a wavelength of $\lambda = 10$ m.

For the numerical diffusion calculation, the diffusivity is taken approximately as a constant over the first metre of firn with a value for δ^{18}O of $D \approx 2.9 \times 10^{-8}\,\mathrm{cm^2\,s^{-1}}$, which has been calculated according to Johnsen et al. (2000) adopting the relevant parameters for Kohnen station. The diffusion length is modeled to vary with time as (Johnsen et al., 2000)

$$\sigma_{\mathrm{diff}}(t) \sim \sqrt{2Dt}\,, \tag{B2}$$

assuming zero vertical strain rate. The time t of burial since deposition is expressed in terms of the depth of the respective snow parcel using the present accumulation rate $\dot{b}$

CPD
11, 5605–5649, 2015

of snow, $t(z) = z/\dot{b}$ with $\dot{b} = 0.2\,\mathrm{m\,yr^{-1}} \approx 6.3 \times 10^{-9}\,\mathrm{m\,s^{-1}}$. In the numerical approach, for each depth $z(t)$ the trench profiles are diffused with respect to the respective diffusion length σ_{diff} by convoluting the original signal with a Gaussian with a standard deviation of $\sigma_{\mathrm{diff}}(t(z))$.

The numerical lateral $\delta^{18}O$ trench variance after diffusion is in qualitatively good agreement with the observational data of trench T1 (Fig. B1).

Acknowledgements. We thank all the scientists, technicians and the logistic support who worked at Kohnen station in the 2012/13 austral summer; especially Melanie Behrens, Tobias Binder, Andreas Frenzel, Katja Instenberg, Katharina Klein, Martin Schneebeli, Jan Tell and Stefanie Weissbach, for assistance in creating the trench dataset. We further thank the technicians of the isotope laboratories in Bremerhaven and Potsdam, especially York Schlomann and Christoph Manthey. All plots and numerical calculations were carried out using the software R: A Language and Environment for Statistical Computing. This work was supported by the Initiative and Networking Fund of the Helmholtz Association Grant VG-NH900.

References

Birnbaum, G., Freitag, J., Brauner, R., König-Langlo, G., Schulz, E., Kipfstuhl, S., Oerter, H., Reijmer, C. H., Schlosser, E., Faria, S. H., Ries, H., Loose, B., Herber, A., Duda, M. G., Powers, J. G., Manning, K. W., and van den Broeke, M. R.: Strong-wind events and their influence on the formation of snow dunes: observations from Kohnen station, Dronning Maud Land, Antarctica, J. Glaciol., 56, 891–902, 2010. 5611

Cuffey, K. M. and Steig, E. J.: Isotopic diffusion in polar firn: implications for interpretation of seasonal climate parameters in ice-core records, with emphasis on central Greenland, J. Glaciol., 44, 273–284, 1998. 5608, 5617

Dansgaard, W.: Stable isotopes in precipitation, Tellus, 16, 436–468, 1964. 5607, 5616

Dansgaard, W., Johnsen, S. J., Clausen, H. B., Dahl-Jensen, D., Gundestrup, N. S., Hammer, C. U., Hvidberg, C. S., Steffensen, J. P., Sveinbjörnsdottir, A. E., Jouzel, J., and Bond, G.: Evidence for general instability of past climate from a 250-kyr ice-core record, Nature, 364, 218–220, doi:10.1038/364218a0, 1993. 5607

CPD
11, 5605–5649, 2015

Ekaykin, A. A., Lipenkov, V. Y., Barkov, N. I., Petit, J. R., and Masson-Delmotte, V.: Spatial and temporal variability in isotope composition of recent snow in the vicinity of Vostok station, Antarctica: implications for ice-core record interpretation, Ann. Glaciol., 35, 181–186, doi:10.3189/172756402781816726, 2002. 5621

EPICA community members: One-to-one coupling of glacial climate variability in Greenland and Antarctica, Nature, 444, 195–198, 2006. 5606, 5609, 5624, 5625

Evans, M. N., Tolwinski-Ward, S. E., Thompson, D. M., and Anchukaitis, K. J.: Applications of proxy system modeling in high resolution paleoclimatology, Quaternary Sci. Rev., 76, 16–28, doi:10.1016/j.quascirev.2013.05.024, 2013. 5616

Fisher, D. A. and Koerner, R. M.: Signal and noise in four ice-core records from the Agassiz Ice Cap, Ellesmere Island, Canada: details of the last millennium for stable isotopes, melt and solid conductivity, Holocene, 4, 113–120, doi:10.1177/095968369400400201, 1994. 5609

Fisher, D. A., Koerner, R. M., Paterson, W. S. B., Dansgaard, W., Gundestrup, N., and Reeh, N.: Effect of wind scouring on climatic records from ice-core oxygen-isotope profiles, Nature, 301, 205–209, doi:10.1038/301205a0, 1983. 5607

Fisher, D. A., Reeh, N., and Clausen, H. B.: Stratigraphic noise in time series derived from ice cores, Ann. Glaciol., 7, 76–83, 1985. 5607, 5609, 5616, 5617

Fujita, K. and Abe, O.: Stable isotopes in daily precipitation at Dome Fuji, East Antarctica, Geophys. Res. Lett., 33, L18503, doi:10.1029/2006GL026936, 2006. 5607

Gfeller, G., Fischer, H., Bigler, M., Schüpbach, S., Leuenberger, D., and Mini, O.: Representativeness and seasonality of major ion records derived from NEEM firn cores, The Cryosphere, 8, 1855–1870, doi:10.5194/tc-8-1855-2014, 2014. 5609, 5622

Graf, W., Oerter, H., Reinwarth, O., Stichler, W., Wilhelms, F., Miller, H., and Mulvaney, R.: Stable-isotope records from Dronning Maud Land, Antarctica, Ann. Glaciol., 35, 195–201, 2002. 5608, 5622

Helsen, M. M., van de Wal, R. S. W., van den Broeke, M. R., Masson-Delmotte, V., Meijer, H. A. J., Scheele, M. P., and Werner, M.: Modeling the isotopic composition of Antarctic snow using backward trajectories: simulation of snow pit records, J. Geophys. Res., 111, D15109, doi:10.1029/2005JD006524, 2006. 5608

Hoshina, Y., Fujita, K., Nakazawa, F., Iizuka, Y., Miyake, T., Hirabayashi, M., Kuramoto, T., Fujita, S., and Motoyama, H.: Effect of accumulation rate on water stable isotopes of near-surface snow in inland Antarctica, J. Geophys. Res., 119, 274–283, doi:10.1002/2013JD020771, 2014. 5608

CPD
11, 5605–5649, 2015

Huntingford, C., Jones, P. D., Livina, V. N., Lenton, T. M., and Cox, P. M.: No increase in global temperature variability despite changing regional patterns, Nature, 500, 327–330, doi:10.1038/nature12310, 2013. 5607

Johnsen, S. J.: Stable isotope homogenization of polar firn and ice, in: Isotopes and Impurities in Snow and Ice, no. 118 in Proceedings of the Grenoble Symposium, IAHS AISH Publ., Grenoble, France, 210–219, 1977. 5608, 5617

Johnsen, S. J., Clausen, H. B., Cuffey, K. M., Hoffmann, G., Schwander, J., and Creyts, T.: Diffusion of stable isotopes in polar firn and ice: the isotope effect in firn diffusion, in: Physics of ice core records, edited by: Hondoh, T., vol. 159, Hokkaido Univ. Press, Sapporo, Japan, 121–140, 2000. 5608, 5617, 5631

Jones, T. R., White, J. W. C., and Popp, T.: Siple Dome shallow ice cores: a study in coastal dome microclimatology, Clim. Past, 10, 1253–1267, doi:10.5194/cp-10-1253-2014, 2014. 5609

Jouzel, J., Alley, R. B., Cuffey, K. M., Dansgaard, W., Grootes, P., Hoffmann, G., Johnsen, S. J., Koster, R. D., Peel, D., Shuman, C. A., Stievenard, M., Stuiver, M., and White, J.: Validity of the temperature reconstruction from water isotopes in ice cores, J. Geophys. Res., 102, 26471–26487, 1997. 5619, 5625

Karlöf, L., Winebrenner, D. P., and Percival, D. B.: How representative is a time series derived from a firn core? A study at a low-accumulation site on the Antarctic plateau, J. Geophys. Res., 111, F04001, doi:10.1029/2006JF000552, 2006. 5608, 5616

Kobashi, T., Kawamura, K., Severinghaus, J. P., Barnola, J.-M., Nakaegawa, T., Vinther, B. M., Johnsen, S. J., and Box, J. E.: High variability of Greenland surface temperature over the past 4000 years estimated from trapped air in an ice core, Geophys. Res. Lett., 38, L21501, doi:10.1029/2011GL049444, 2011. 5607

Laepple, T. and Huybers, P.: Reconciling discrepancies between Uk37 and Mg/Ca reconstructions of Holocene marine temperature variability, Earth Planet. Sc. Lett., 375, 418–429, doi:10.1016/j.epsl.2013.06.006, 2013. 5607, 5616, 5624

Laepple, T. and Huybers, P.: Ocean surface temperature variability: large model–data differences at decadal and longer periods, P. Natl. Acad. Sci. USA, 111, 16682–16687, doi:10.1073/pnas.1412077111, 2014. 5607

Laepple, T., Werner, M., and Lohmann, G.: Synchronicity of Antarctic temperatures and local solar insolation on orbital timescales, Nature, 471, 91–94, doi:10.1038/nature09825, 2011. 5617

CPD
11, 5605–5649, 2015

Legrand, M. and Mayewski, P.: Glaciochemistry of polar ice cores: a review, Rev. Geophys., 35, 219–243, doi:10.1029/96RG03527, 1997. 5607

McMorrow, A. J., Curran, M. A. J., Van Ommen, T. D., Morgan, V. I., and Allison, I.: Features of meteorological events preserved in a high-resolution Law Dome (East Antarctica) snow pit, Ann. Glaciol., 35, 463–470, doi:10.3189/172756402781816780, 2002. 5609

Mosley-Thompson, E., McConnell, J. R., Bales, R. C., Li, Z., Lin, P.-N., Steffen, K., Thompson, L. G., Edwards, R., and Bathke, D.: Local to regional-scale variability of annual net accumulation on the Greenland ice sheet from PARCA cores, J. Geophys. Res., 106, 33839–33851, doi:10.1029/2001JD900067, 2001. 5607

NEEM community members: Eemian interglacial reconstructed from a Greenland folded ice core, Nature, 493, 489–494, doi:10.1038/nature11789, 2013. 5623

Neumann, T. A. and Waddington, E. D.: Effects of firn ventilation on isotopic exchange, J. Glaciol., 50, 183–194, 2004. 5608, 5617, 5618

Oerter, H., Graf, W., Meyer, H., and Wilhelms, F.: The EPICA ice core from Dronning Maud Land: first results from stable-isotope measurements, Ann. Glaciol., 39, 307–312, 2004. 5624

Persson, A., Langen, P. L., Ditlevsen, P., and Vinther, B. M.: The influence of precipitation weighting on interannual variability of stable water isotopes in Greenland, J. Geophys. Res., 116, D20120, doi:10.1029/2010JD015517, 2011. 5608, 5617

Petit, J. R., Jouzel, J., Raynaud, D., Barkov, N. I., Barnola, J.-M., Basile, I., Bender, M., Chappellaz, J., Davis, M., Delaygue, G., Delmotte, M., Kotlyakov, V. M., Legrand, M., Lipenkov, V. Y., Lorius, C., Pépin, L., Ritz, C., Saltzman, E., and Stievenard, M.: Climate and atmospheric history of the past 420,000 years from the Vostok ice core, Antarctica, Nature, 399, 429–436, doi:10.1038/20859, 1999. 5607

Raynaud, D., Jouzel, J., Barnola, J.-M., Chappellaz, J., Delmas, R. J., and Lorius, C.: The ice record of greenhouse gases, Science, 259, 926–934, doi:10.1126/science.259.5097.926, 1993. 5606

Rehfeld, K., Marwan, N., Heitzig, J., and Kurths, J.: Comparison of correlation analysis techniques for irregularly sampled time series, Nonlin. Processes Geophys., 18, 389–404, doi:10.5194/npg-18-389-2011, 2011. 5615

Richardson, C., Aarholt, E., Hamran, S.-E., Holmlund, P., and Isaksson, E.: Spatial distribution of snow in western Dronning Maud Land, East Antarctica, mapped by a ground-based snow radar, J. Geophys. Res., 102, 20343–20353, doi:10.1029/97JB01441, 1997. 5617

CPD
11, 5605–5649, 2015

Sime, L. C., Marshall, G. J., Mulvaney, R., and Thomas, E. R.: Interpreting temperature information from ice cores along the Antarctic Peninsula: ERA40 analysis, Geophys. Res. Lett., 36, L18801, doi:10.1029/2009GL038982, 2009. 5608, 5617

Sime, L. C., Lang, N., Thomas, E. R., Benton, A. K., and Mulvaney, R.: On high-resolution sampling of short ice cores: dating and temperature information recovery from Antarctic Peninsula virtual cores, J. Geophys. Res., 116, D20117, doi:10.1029/2011JD015894, 2011. 5608, 5617

Sommer, S., Appenzeller, C., Röthlisberger, R., Hutterli, M. A., Stauffer, B., Wagenbach, D., Oerter, H., Wilhelms, F., Miller, H., and Mulvaney, R.: Glacio-chemical study spanning the past 2 kyr on three ice cores from Dronning Maud Land, Antarctica: 1. Annually resolved accumulation rates, J. Geophys. Res., 105, 29411–29421, doi:10.1029/2000JD900449, 2000a. 5608

Sommer, S., Wagenbach, D., Mulvaney, R., and Fischer, H.: Glacio-chemical study spanning the past 2 kyr on three ice cores from Dronning Maud Land, Antarctica: 2. Seasonally resolved chemical records, J. Geophys. Res., 105, 29423–29433, 2000b. 5608

Steen-Larsen, H. C., Masson-Delmotte, V., Sjolte, J., Johnsen, S. J., Vinther, B. M., Bréon, F.-M., Clausen, H. B., Dahl-Jensen, D., Falourd, S., Fettweis, X. Gallée, H., Jouzel, J., Kageyama, M., Lerche, H., Minster, B., Picard, G., Punge, H. J., Risi, C., Salas, D., Schwander, J., Steffen, K., Sveinbjörnsdóttir, A. E., Svensson, A., and White, J.: Understanding the climatic signal in the water stable isotope records from the NEEM shallow firn/ice cores in northwest Greenland, J. Geophys. Res., 116, D06108, doi:10.1029/2010JD014311, 2011. 5609

Steen-Larsen, H. C., Masson-Delmotte, V., Hirabayashi, M., Winkler, R., Satow, K., Prié, F., Bayou, N., Brun, E., Cuffey, K. M., Dahl-Jensen, D., Dumont, M., Guillevic, M., Kipfstuhl, S., Landais, A., Popp, T., Risi, C., Steffen, K., Stenni, B., and Sveinbjörnsdottír, A. E.: What controls the isotopic composition of Greenland surface snow?, Clim. Past, 10, 377–392, doi:10.5194/cp-10-377-2014, 2014. 5608, 5617

Steig, E. J.: Sources of uncertainty in ice core data, available at: http://ftp.pages-igbp.org/products/meeting-products/2030-white-paper-sources-of-uncertainty-in-ice-core-data (last access: 24 November 2015), a contribution to the workshop on Reducing and Representing Uncertainties in High-Resolution Proxy Data, International Centre for Theoretical Physics, Trieste, Italy, 9–11 June 2008, 2009. 5616

CPD
11, 5605–5649, 2015

Steig, E. J., Schneider, D. P., Rutherford, S. D., Mann, M. E., Comiso, J. C., and Shindell, D. T.: Warming of the Antarctic ice-sheet surface since the 1957 International Geophysical Year, Nature, 457, 459–462, doi:10.1038/nature07669, 2009. 5624

Town, M. S., Warren, S. G., von Walden, P., and Waddington, E. D.: Effect of atmospheric water vapor on modification of stable isotopes in near-surface snow on ice sheets, J. Geophys. Res., 113, D24303, doi:10.1029/2008JD009852, 2008. 5608, 5617, 5618

van Geldern, R. and Barth, J. A. C.: Optimization of instrument setup and post-run corrections for oxygen and hydrogen stable isotope measurements of water by isotope ratio infrared spectroscopy (IRIS), Limnol. Oceanogr.-Meth., 10, 1024–1036, doi:10.4319/lom.2012.10.1024, 2012. 5610

Waddington, E. D., Steig, E. J., and Neumann, T. A.: Using characteristic times to assess whether stable isotopes in polar snow can be reversibly deposited, Ann. Glaciol., 35, 118–124, 2002. 5608, 5617, 5618

Whillans, I. M. and Grootes, P. M.: Isotopic diffusion in cold snow and firn, J. Geophys. Res., 90, 3910–3918, doi:10.1029/JD090iD02p03910, 1985. 5608, 5617

Wigley, T. M. L., Briffa, K. R., and Jones, P. D.: On the average value of correlated time series, with applications in dendroclimatology and hydrometeorology, J. Clim. Appl. Meteorol., 23, 201–213, doi:10.1175/1520-0450(1984)023<0201:OTAVOC>2.0.CO;2, 1984. 5620, 5622

CPD
11, 5605–5649, 2015

Table 1. The variance levels observed for the two trenches: The lateral variance is the mean horizontal variance over all depth layers, the down-core variance gives the mean vertical variance over all respective trench profiles. The seasonal as well as the inter-annual variance levels denote the variances of the respective mean seasonal and inter-annual $\delta^{18}O$ time series of the two trenches (Fig. 6). All numbers are in units of $(‰)^2$.

trench	lateral σ_l^2	down-core σ_v^2	seasonal $\overline{\sigma}_v^2$	inter-annual $\overline{\sigma}_a^2$
T1	5.9	9.5	5.1	1.15
T2	5.3	7.3	3.3	0.21

CPD
11, 5605–5649, 2015

Table 2. The noise variance and standard deviation (SD) of the trench data and the ratio of the measurement uncertainty ($\Delta\delta^{18}O = 0.09‰$) and the respective noise SD, given for different time scales and for the two scenarios of the annual noise variance.

time scale	variance in $(‰)^2$	SD in ‰	$\Delta\delta^{18}O/SD$
seasonal	5.9	2.43	4 %
annual: case I	1.25	1.12	8 %
annual: case II	5.9	2.43	4 %
10 yr-avg.: case I	0.13	0.36	25 %
10 yr-avg.: case II	0.59	0.77	12 %

CPD
11, 5605–5649, 2015

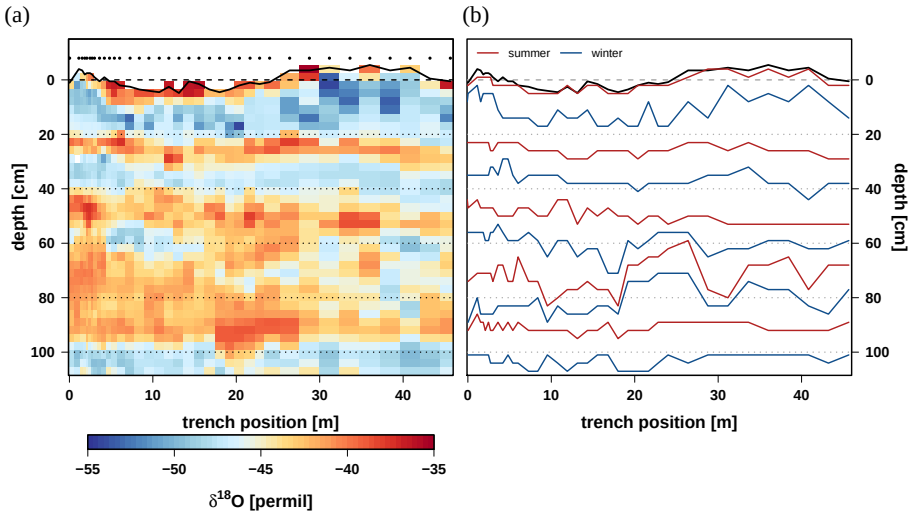

Figure 1. (a) The two-dimensional δ^{18}O profile of trench T1. The depth scale is relative to the mean snow height (long-dashed black line); the solid black line shows the local snow height at the sampling positions which are indicated by black dots above the snow profile. White gaps indicate missing data. **(b)** The stratigraphy of trench T1 expressed as the seasonal layer profiles by tracking the local δ^{18}O extrema.

CPD
11, 5605–5649, 2015

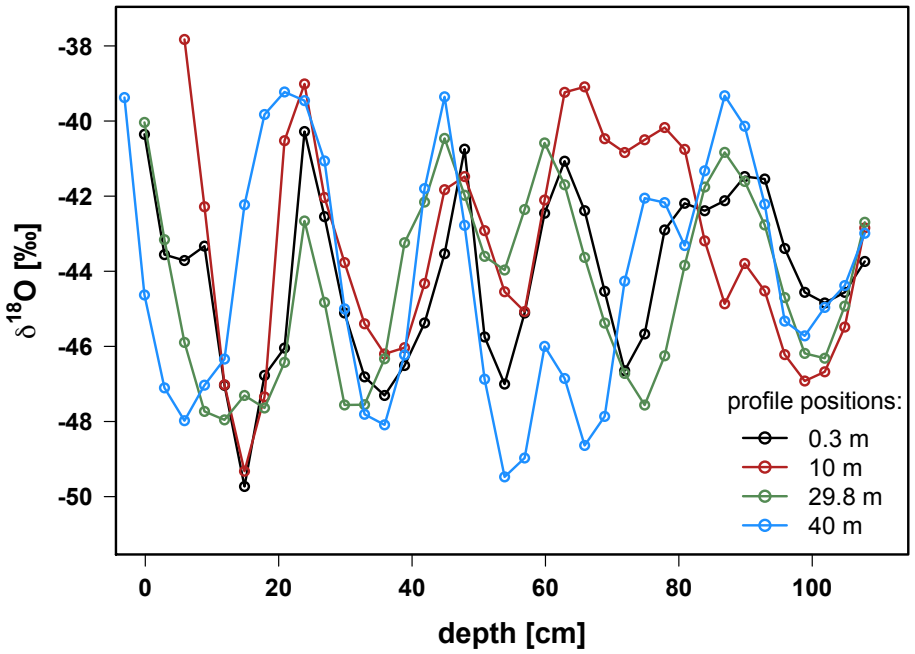

Figure 2. The four isotope profiles from trench T2 as a function of depth below the mean snow height.

CPD
11, 5605–5649, 2015

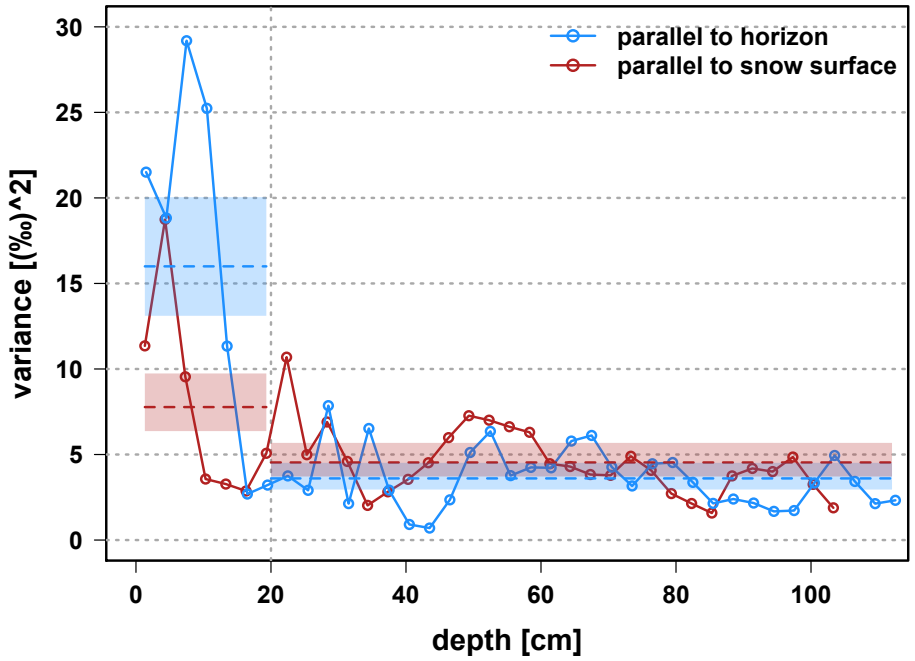

Figure 3. The lateral variance of T1 as a function of depth below the mean snow height. Blue lines with circles give the lateral variance as calculated horizontally, red lines with circles display the variance computed for consecutive slices following the present snow surface. Dashed horizontal lines show the mean variance of each variance profile for the depth ranges of 0–20 and 20– ~ 110 cm where the shadings represent the 90 % confidence intervals of the respective mean.

CPD
11, 5605–5649, 2015

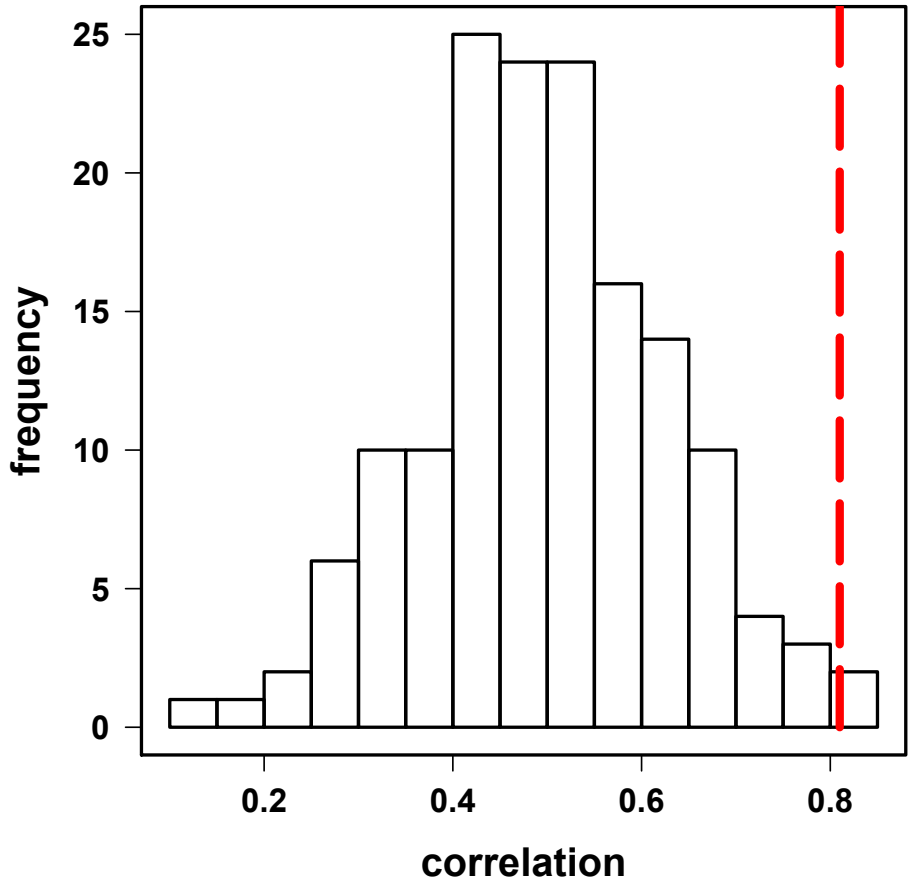

Figure 4. Histogram of all possible pairwise correlations (N = 152) between single profiles of trench T1 and single profiles of trench T2. Displayed are the maximum correlations allowing vertical shifts of the T2 profiles of up to ±12 cm. Shown as a red line is the correlation between the mean δ^{18}O profile of T1 and the mean δ^{18}O profile of T2 (Fig. 6).

CPD
11, 5605–5649, 2015

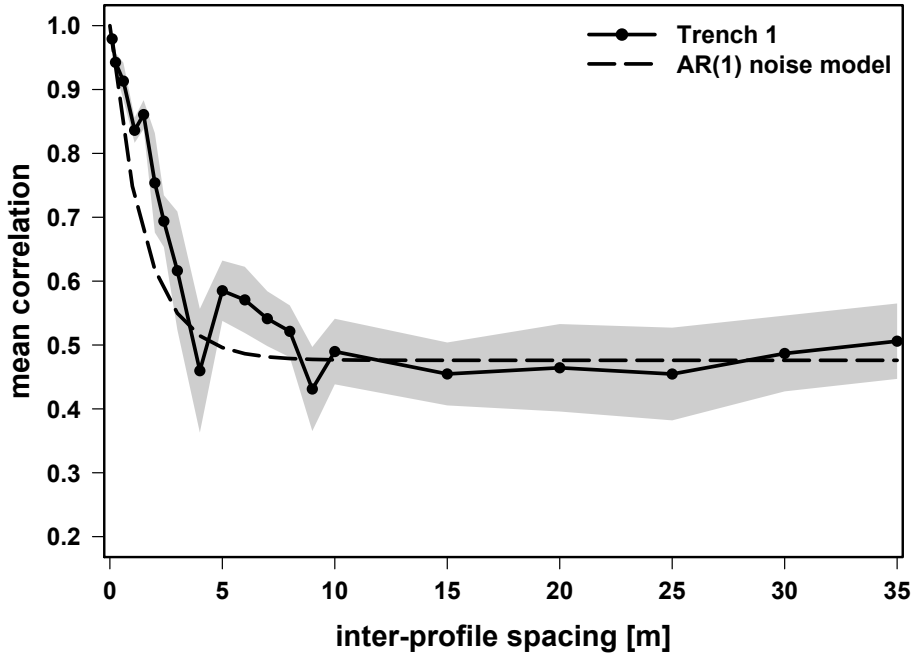

Figure 5. The mean inter-profile correlation as a function of profile spacing for T1 (black line with filled circles). Shadings denote the standard error of the mean (undefined if just one profile pair is found for a given spacing), for each spacing calculated adopting an effective number of profile pairs that is set to the lower value of the actually found number of pairs and the effective degrees of freedom for the trench record in lateral direction. The dashed black line denotes the theoretical inter-profile correlation calculated for first-order autoregressive noise (AR(1)).

CPD
11, 5605–5649, 2015

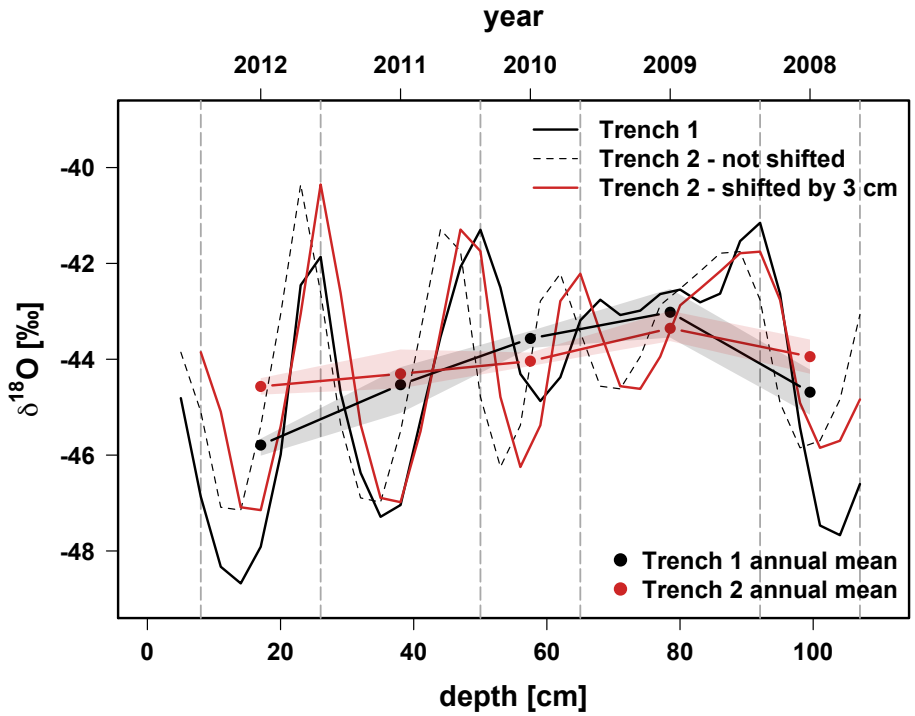

Figure 6. Comparison of the mean seasonal $\delta^{18}O$ profiles as a function of depth below the mean snow height obtained from trench T1 (black solid line) and T2 (red solid line). Vertical shifting of ±12 cm was allowed to maximise the correlation, resulting in a shift of +3 cm of the original T2 mean profile (black dashed line). The mean profiles are well correlated with $r_{T1,T2}$ = 0.81. Additionally, red and black points with lines give the approximate annual-mean $\delta^{18}O$ time series for the trenches. Shadings represent the range due to different binning definitions. Note that the first and last value of the annual-mean time series (years 2012 and 2008) are biased since the trench data are incomplete here. The vertical dashed grey lines are the positions of the six local maxima of the average profile obtained from the trench mean profiles.

CPD
11, 5605–5649, 2015

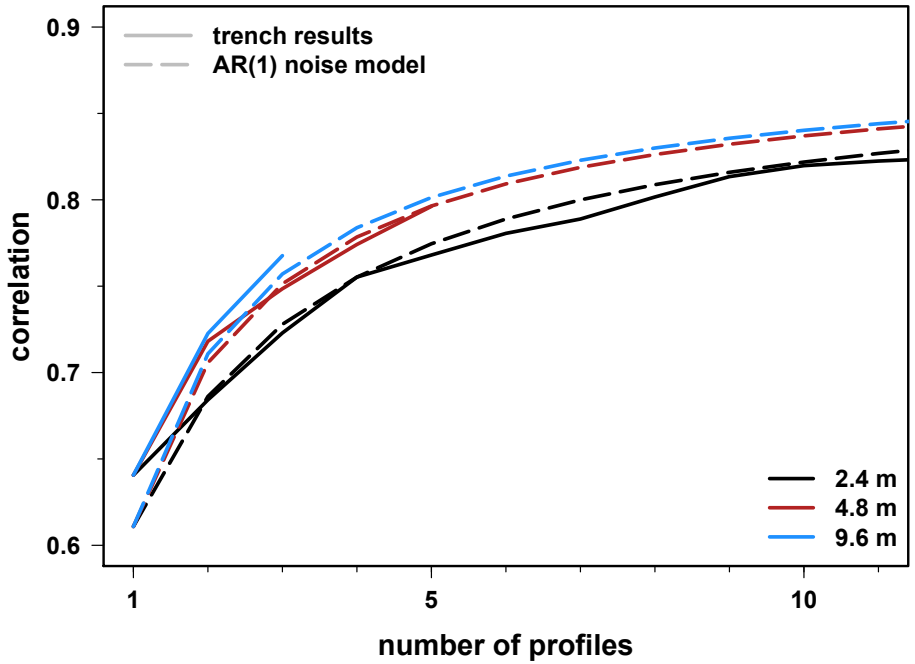

Figure 7. The correlation between a set of averaged T1 profiles and the mean of all T2 profiles depending on the number of profiles in the T1 set and their inter-profile spacing. Three different spacings are investigated: 2.4 m (black), 4.8 m (red) and 9.6 m (blue). Solid lines show the results for the actual trench data, dashed lines display the theoretical correlations calculated for AR(1) autoregressive noise. The trench results are given as the mean of the correlations obtained for all possible unique sets of profiles separated by the given spacing and are only calculated when at least 15 sets are available.

CPD
11, 5605–5649, 2015

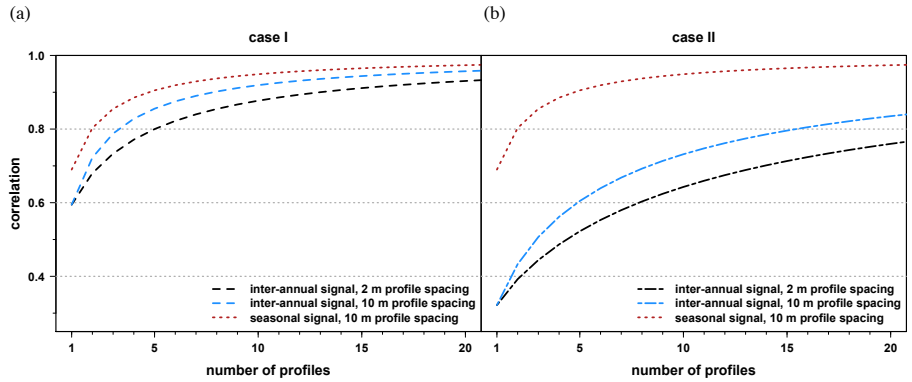

Figure 8. The representativity of an average set of δ^{18}O firn profiles expressed as the correlation with a hypothetical regional climate signal depending on the number of profiles averaged as well as their inter-profile spacing. The dashed red line shows the representativity on the seasonal time scale for 10 m profile spacing. For the inter-annual time scale, the two limiting cases discussed in the text are displayed (**a**: best-case scenario/case I, **b**: worst-case scenario/case II), each for 2 m profile spacings (black) as well as 10 m profile spacings (blue).

CPD
11, 5605–5649, 2015

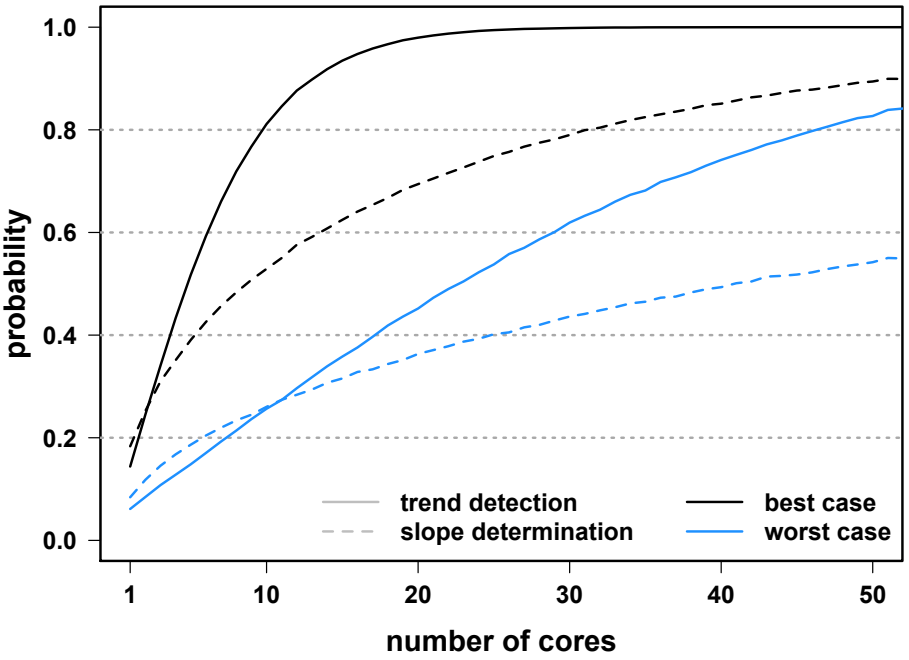

Figure 9. The probability of detecting a linear temperature trend of 0.5 °C/50 yr (correlation > 0, $p \geq 0.05$) (solid lines) and of determining the strength of the trend with an accuracy of 25 % (dashed lines), each as a function of the number of annually resolved firn cores averaged and for the two scenarios of the annual noise variance discussed in the text (black lines: best case/case I, blue lines: worst case/case II).

CPD
11, 5605–5649, 2015

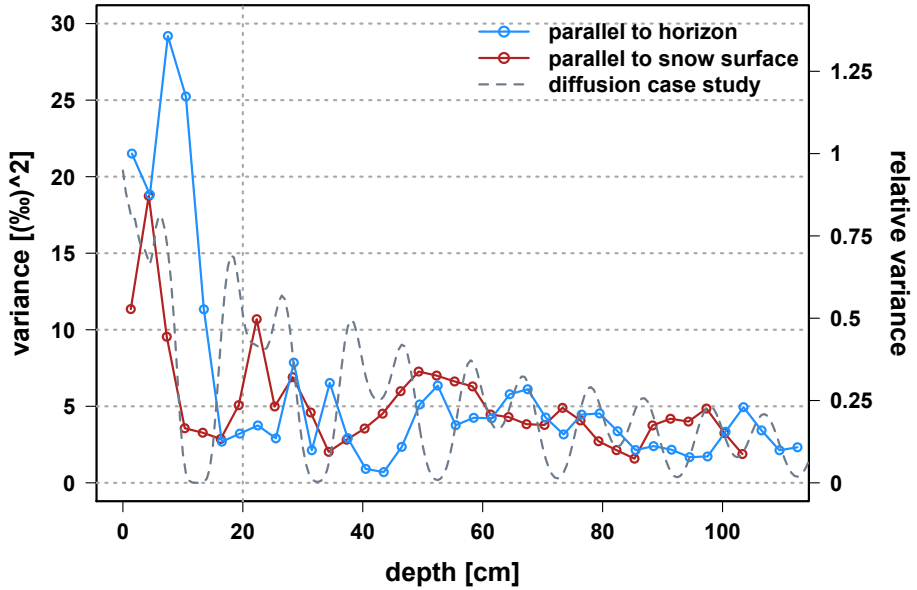

Figure B1. The lateral variance of T1 as a function of depth below the mean snow height. Blue lines with circles give the lateral variance as calculated horizontally, red lines with circles display the variance computed for consecutive slices following the present snow surface. Greyish-blue dashed lines depict the numerical estimate of the vertical variance of a diffused artificial trench record (see text for details).

CPD
11, 5605–5649, 2015